International Journal of Nanoelectronics and Materials
Volume 13 (Special Issue) Dec 2020 (301-308)

First-Principles Calculations on Structural, Electronic and Optical Properties of Ce-, Nd- and Er-doped TiO_2

M. H. Samat[4], M. F. M. Taib[1,4], O. H. Hassan[2, 4], M. Z. A. Yahya[3, 4] and A. M. M. Ali[1, 4*]

[1]*Faculty of Applied Sciences, Universiti Teknologi MARA (UiTM), 40450 Shah Alam, Selangor, Malaysia.*
[2]*Department of Industrial Ceramics, Faculty of Art & Design, Universiti Teknologi MARA (UiTM), 40450 Shah Alam, Selangor, Malaysia.*
[3]*Faculty of Defence Science & Technology, Universiti Pertahanan Nasional Malaysia, 57000 Kuala Lumpur, Malaysia.*
[4]*Ionic Materials & Devices (iMADE) Research Laboratory, Institute of Science, Universiti Teknologi MARA (UiTM), 40450 Shah Alam, Selangor, Malaysia.*

ABSTRACT

In this work, the first-principles calculations on the structural, electronic and optical properties of lanthanides (Ln)-doped anatase TiO_2 using Ln elements from cerium (Ce), neodymium (Nd) and erbium (Er) were performed to observe the effects of Ln doping that can improve the properties of TiO_2. The Ln-doped TiO_2 has lower band gaps compared to pure TiO_2 due to the presence of impurity energy levels (IELs) from Ln 4f states which can be seen from the density of states (DOS). Among the Ln-doped TiO_2, the shift of light towards a longer wavelength spectrum is from Nd-doped TiO_2. Overall, the first-principles study from the deepest atomic level in this work can clarify the Ln doping effects in TiO_2.

Keywords: First-Principles, Dye-Sensitized Solar Cells, TiO_2, Lanthanide, Optical Properties.

1. INTRODUCTION

Titanium dioxide (TiO_2) occurs naturally in three distinct forms which are rutile, anatase and brookite. TiO_2 has excellent properties such as low cost, non-toxicity, chemical stability and high oxidizing power [1]. TiO_2 found in all kinds of applications such as air and water purification, offset printing, agriculture, medical, energy conversion and water splitting [2]. Anatase TiO_2, as one of the most well-known functional materials, is widely used in numerous fields of the environment and energy compared to other TiO_2 phases [3]. However, anatase TiO_2 can only be activated under the ultraviolet (UV) radiation from the sunlight due to its wider energy band gap (~3.2) where the energy of UV light only corresponds to about 3-5%. Generally, sunlight consist of almost 4% of UV light and 43% of visible light. This indicates that TiO_2 can be activated in a small portion of the solar energy, leading to its quite low solar energy usage.

Among various methods of modifying TiO_2 for the utilization of longer wavelength spectrum such as metal and non-metal doping [4], noble metal deposition [5] and sensitization by inorganic complexes or organic dyes [6], doping with a metal element from Ln is considered as one of the effective methods. The Ln-doped TiO_2 have been studied extensively because of their unique 4*f* electron configuration [7–9].

From the previous experimental reports, Ce-, Nd- and Er-doped TiO_2 show great improvement as photoanodes of dye-sensitized solar cell (DSSC) and photocatalyst over pure TiO_2 [10-15]. However, the structural, electronic and optical properties of these Ln dopants (Ce, Nd and Er) in TiO_2 using density functional theory (DFT) did not intensively investigated yet. Hence, some

*Corresponding Author: *ammali@uitm.edu.my*

questions involving the effect of the Ce, Nd and Er dopants in TiO_2 need to be theoretically clarified.

In this work, the aim is to determine the effect of lanthanide (Ln) dopants (Ln = Ce, Nd and Er) on structural (lattice parameters, volume, bond length) electronic (band structures, total and partial density of states) and optical (absorption coefficient) properties of TiO_2 using first-principles calculations within DFT framework.

2. COMPUTATIONAL METHOD

The Ln-doped anatase TiO_2 using Ce, Nd and Er as Ln dopants were constructed by replacing one Ti atom with the Ln atoms at (0.5, 0.5, 0.5) of atomic position. The structural, electronic and optical properties of the Ln-doped TiO_2 were calculated using the exchange-correlation functional from generalized gradient approximation by Perdew-Burke-Ernzerhof for solids (GGA-PBEsol) [16] within Cambridge Serial Total Energy Package (CASTEP) [17] software. The cut-off energy of 410 eV, 440 eV and 380 eV were used for Ce-, Nd- and Er-doped TiO_2, respectively while the *k*-points sampling of 4×4×2 was set in Monkhorst-Pack grid for the Ln-doped TiO_2. The pseudo atomic calculation for Ti and O was represented by 3*s* 3*p* 3*d* 4*s* and 2*s* 2*p*, respectively while for Ln is 4*f* 5*s* 5*p* 6*s*. The geometrical optimization was set using 5.0×10^{-6} eV/atom for total energy, 0.01 eV/Å for maximum force, 0.02 GPa for maximum stress and 5.0×10^{-4} Å for maximum displacement. As widely known, the DFT calculation usually underestimates the band gap for *d* and *f* orbitals. However, the inclusion of +U term was found to be unessential to clarify the difference between Ce-, Nd- and Er-doped TiO_2 since this work only concentrates on the impact of the Ln dopants on the properties of TiO_2.

3. RESULTS AND DISCUSSION

3.1.1 Structural Properties

The structural properties of pure TiO_2, Ce-, Nd- and Er-doped TiO_2 were investigated by optimizing each crystal structure. The Ce-, Nd- and Er-doped TiO_2 were built by replacing Ti atom with Ce, Nd and Er atoms as visualized in Figure 1. To investigate the changes of the geometrical structure caused by the Ln dopants, the optimized cell parameters for the pure TiO_2 and Ln-doped TiO_2 were compared. The structural parameters of the pure TiO_2 and Ln-doped TiO_2 are listed in Table 1. The obtained lattice parameters (*a*, *b* and *c*) and unit cell volume (V) of TiO_2 in this wok are agreed with experimental reports [18, 19] and other theoretical calculations [20, 21]. Thus, the calculations method in this work is reasonable to be performed. It was found that the lattice parameters and volume of the Ln-doped TiO_2 are larger than those of the pure TiO_2. This is due to the incorporation of the Ln ions into TiO_2 lattice to become more distorted by the Ln atoms impurity. The lattice constant along with *c* parameter is larger than *a* and *b* parameters for the pure TiO_2 and Ln-doped TiO_2. It can be seen that the lattice parameters of Ce-, Nd- and Er-doped TiO_2 were overestimated by 3.05%, 3.26% and 2.73% (*a* = *b* parameters) and 6.04%, 4.36% and 3.04% (*c* parameter) over pure TiO_2. Compared with the volume of pure TiO_2, the Ln dopants of Ce, Nd and Er in TiO_2 expand their unit cell volumes by 12.56%, 11.23% and 8.75%, respectively. This is because, the atomic radius of Ce (1.85 Å), Nd (2.06 Å) and Er (2.26 Å) are larger than Ti (1.76 Å) [22].

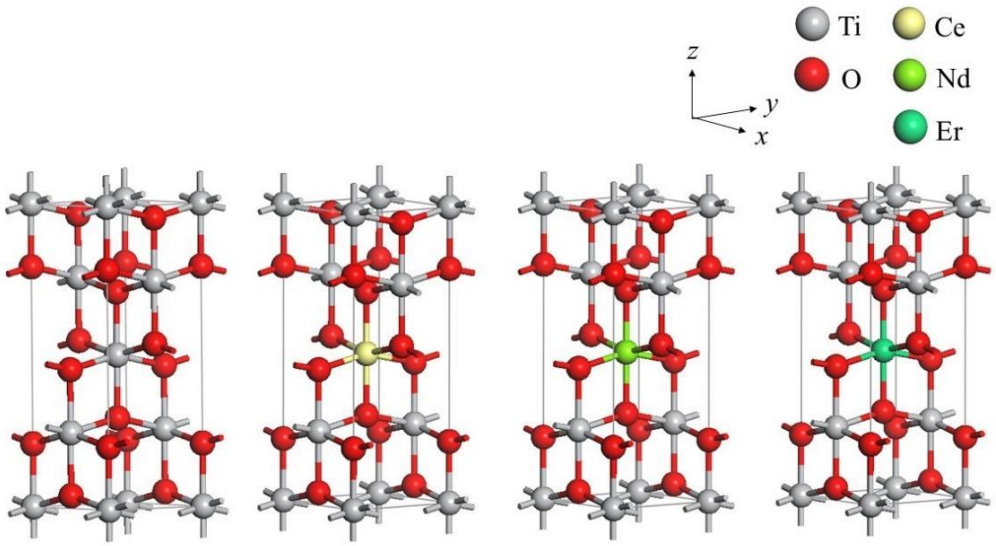

Figure 1. Crystal structures of pure TiO_2, Ce- Nd- and Er-doped TiO_2.

Table 1 Structural parameters of pure TiO_2 and Ce-, Nd- and Er-doped TiO_2

	Pure TiO_2	**Ce-doped TiO_2**	**Nd-doped TiO_2**	**Er-doped TiO_2**
***a* (Å)**	3.775	3.890 (+3.05%)	3.898 (+3.26%)	3.878 (+2.73%)
***b* (Å)**	3.775	3.890 (+3.05%)	3.898 (+3.26%)	3.878 (+2.73%)
***c* (Å)**	9.574	10.152 (+6.04%)	9.991 (+4.36%)	9.865 (+3.04%)
V (Å^3)	2.536	2.610 (+2.92%)	2.563 (+1.06%)	2.544 (+0.32%)

(+) overestimation compared to pure TiO_2

The average bond length of pure TiO_2 and Ln-doped TiO_2 for Ti-O, O-O and Ln-O bonds are listed in Table 2. The O-O bonds are longer compared to Ti-O and Ln-O bonds while the Ti-O bond lengths after Ln doping are slightly elongated than the Ti-O bond lengths before doping. The Ln-O bond for Ce-O (2.262 Å), Nd-O (2.222 Å) and Er-O (2.174 Å) are quite longer than Ti-O bond (1.959) by +0.36%, +0.26% and +0.10% overestimation, suggesting that the Ln-O bond have weaker covalency than Ti-O bond. It should be noted that the longer bond length leads to a weaker bond strength. In general, the increase of bond length between cation and anion may decrease the coupling constant and consequently decrease the band gap according to spectroscopic analysis of a set of tetrahedrally coordinated semiconductors [23]. The calculations on lattice parameters from the previous report for the Ce-doped TiO_2 photoanode by Zhang et al. [24] revealed the expansion of the lattice parameter of TiO_2 when doped with Ce dopant.

Table 2 Average bond length in pure TiO_2 and Ce-, Nd- and Er-doped TiO_2

	Pure TiO_2	**Ce-doped TiO_2**	**Nd-doped TiO_2**	**Er-doped TiO_2**
Ti-O (Å)	1.959	1.966 (+0.36%)	1.964 (+0.26%)	1.961 (+0.10%)
O-O (Å)	2.626	2.657 (+1.18%)	2.659 (+1.26%)	2.651 (+0.95%)
Ln-O (Å^3)	-	2.262	2.222	2.174

(+) overestimation compared to pure TiO_2

3.1.2 Electronic Properties

The incorporation of Ln atoms in anatase TiO_2 not only influences the structural properties but also affects its electronic properties. The band structures of pure TiO_2 and Ce-, Nd- and Er-doped TiO_2 are shown in Figure 2. When the Ln elements are doped in TiO_2, the band gaps are narrower than pure TiO_2. The band gap of pure TiO_2 is 2.127 eV while the band gaps of Ce-, Nd- and Er-doped TiO_2 reduce to 2.065 eV, 1.273 eV and 1.562 eV, respectively. The band gap of anatase is consistent with other finding [25-27], but underestimated the experimental band gap [28, 29]. This is due to the electrons living in the localized orbitals experience strong correlations among each other with a subtle coupling to the extended *s-p* states. This causes a complicated many-electron problem that might not well represented DFT [30].

The reduction of the band gaps of Ln-doped TiO_2 is due to the additional Ln 4*f* states from Ce 4*f*, Nd 4*f* and Er 4*f* which can be seen in the density of states (DOS). The decrease in band gap could also be corroborated with the fact of the increase in crystallite size and particle size after doping as the statement from V. I. Klimov "size-dependent control to energy gap is simply proportional to $1/r^2$" (where *r* is the particle radius) [31].

The top of the valence band exhibited no movement for Ce- and Nd-doped TiO_2, except for Er-doped TiO_2. For the bottom of the conduction band of the Ln-doped TiO_2, there is shift of the band to the lower energy region compare to pure TiO_2. From the comparison on the band structures between the Ln-doped TiO_2, the Ce doping shows the weak influence on the energy structure of TiO_2 from its higher band gaps compared to others Ln dopants where its band gap reduced by 2.91% while the band gaps of Nd- and Er-doped TiO_2 reduced by 40.5% and 26.6%, respectively. The Nd-doped TiO_2 turned out to have the lowest band gap compared to Ce- and Er-doped TiO_2. There is also an impurity energy level (IEL) that appears in the middle of the band gap of Nd-doped TiO_2. Therefore, the electrons in the valence band can be excited to the IEL and then subsequently excited to the conduction band by the visible light irradiation. So, the IEL is beneficial for extending the sensitive light wavelength. The narrower band gap expands the response in the visible region and increases the utilization percentage of sunlight. The narrower band gap also increase the opportunity of an electron to migrate from valence band to conduction band.

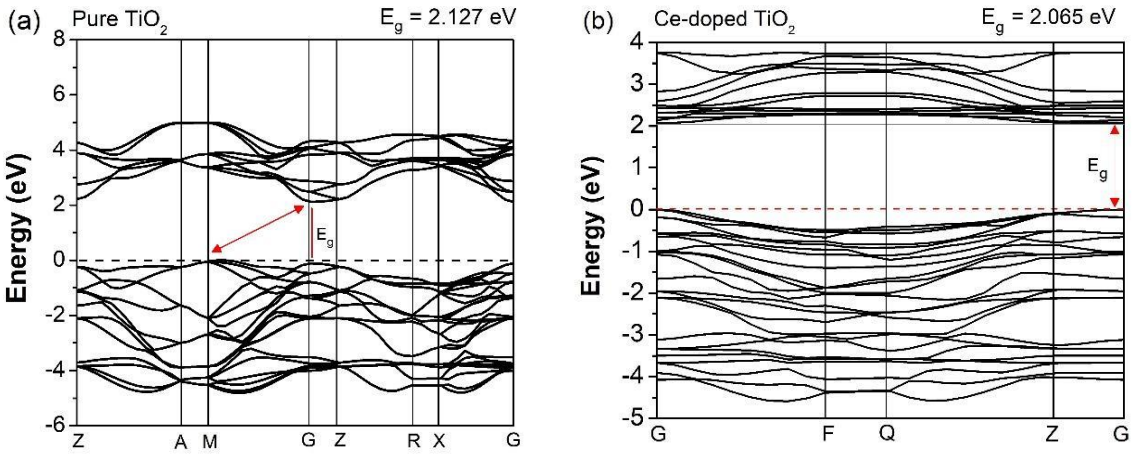

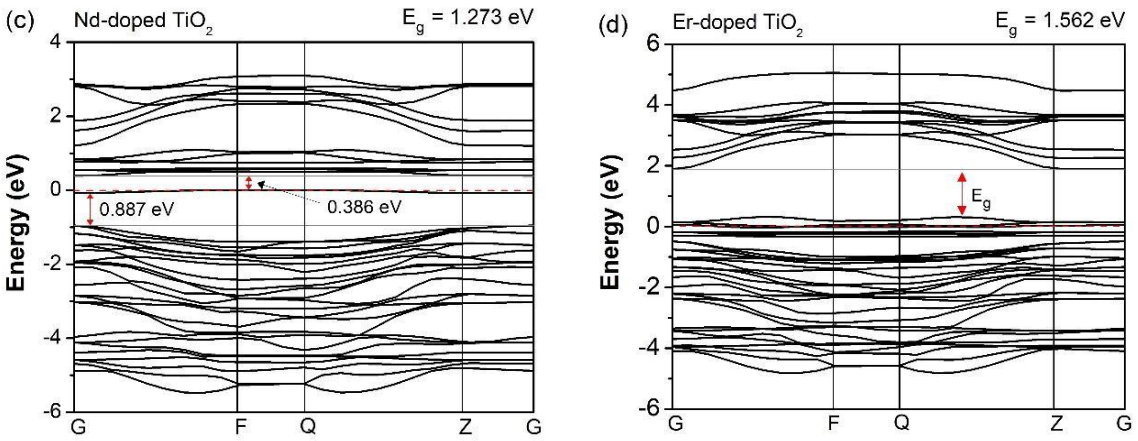

Figure 2. Band structures of (a) pure TiO_2, (b) Ce- (c) Nd- and (d) Er-doped TiO_2.

The total and partial density of states (DOS) of pure TiO_2 and Ce-, Nd- and Er-doped TiO_2 are shown in Figure 3. In pure TiO_2, the valence band and conduction band consist of both O 2*p* and Ti 3*d* states. However, for the Ln-doped TiO_2, there are impurity energy levels (IELs) which consist of the Ln 4*f* states from Ce 4*f*, Nd 4*f* and Er 4*f*. These impurity states would be expected to modify the valence band and the conduction band of the TiO_2. After the presence of the Ln doping, the band gaps of TiO_2 are narrow due to the additional states from the Ln 4*f* states. From the DOS of Ln-doped TiO_2, it can be concluded that the absorption edge transition occurs between O 2*p* and Ce 4*f*, Nd 4*f* or Er 4*f* states instead of Ti 3*d* state.

In the case of the Ce-doped TiO_2, the IEL from the Ce 4*f* state dominate the conduction band which is located close to the bottom of the conduction band while no obvious appearance of Ce 4*f* state at the valence band. This is consistent with the result of X-ray photoelectron spectroscopy valence band (XPS-VB) spectra of the Ce-doped photoanode performed by Zhang et al. [24] to investigate the influence of Ce modification on the valence band of the TiO_2. The XPS-VB spectra of the Ce-doped TiO_2 with different Ce concentrations keep unchanged as the pure TiO_2, indicating Ce doping did not introduce any impurity states near the valence band edge of the nanocrystal. The location of IEL of Ce atom at the bottom of the conduction band made the IEL becomes a shallow donor level. This kind of IEL could act as trap center for photoexcited holes or electrons which could reduce the recombination rate.

For the Nd-doped TiO_2, the substitutional Nd atom to Ti atom results in the overlapping of the Nd 4*f* states which occurs in the middle of the band gap (intermediate level) and at the conduction band minimum (CBM). Due to the crystal imperfections after Nd doping, the periodic potential field is destroyed and additional energy levels are generated in the forbidden gap. In the case of the intermediate level, if the photon energy is absorbed, the electrons in the valence band will first be excited to the new states (impurity states) and finally excited to the conduction band. This may reduce the energy required for electron transition, lower the threshold of photoexcitation and expand the optical absorption spectrum without reducing the energy of electrons or holes. This can greatly improve the light conversion efficiency of TiO_2. However, the impurity states near the middle of the band gap are deep impurity states. These deep impurity states can easily become the recombination centers of the photoexcited electron-hole pairs, especially at high doping concentration structures. However, in the case of IEL at CBM, it could act as trap centre for photoexcited electrons which could reduce the recombination rate of charge carriers.

As for the Er-doped TiO_2, the IEL formed by Er 4*f* state is located above the valence band near the Fermi level and partially overlaps with the valence band maximum (VBM). This kind of IEL could reduce the recombination rate of the charge carriers (electrons and holes) because shallow

acceptor of Er 4*f* state would act as a trap center for photoexcited holes, which is beneficial for photoexcitation charge carriers' migration. Because the Er-doped TiO_2 level is close to the valence band, the holes easily overlap in the highly impurity of Er dopants.

Therefore, this finding on the DOS of Ln-doped TiO_2 indicates that the Ln doping induces impurity states originates from the 4*f* electrons that tune the location of valence band and conduction bands. The effect of the band change will lead to the increasing visible light absorption. This result gives a good explanation of the red shift of the light absorption in Ln-doped TiO_2 compare to pure TiO_2.

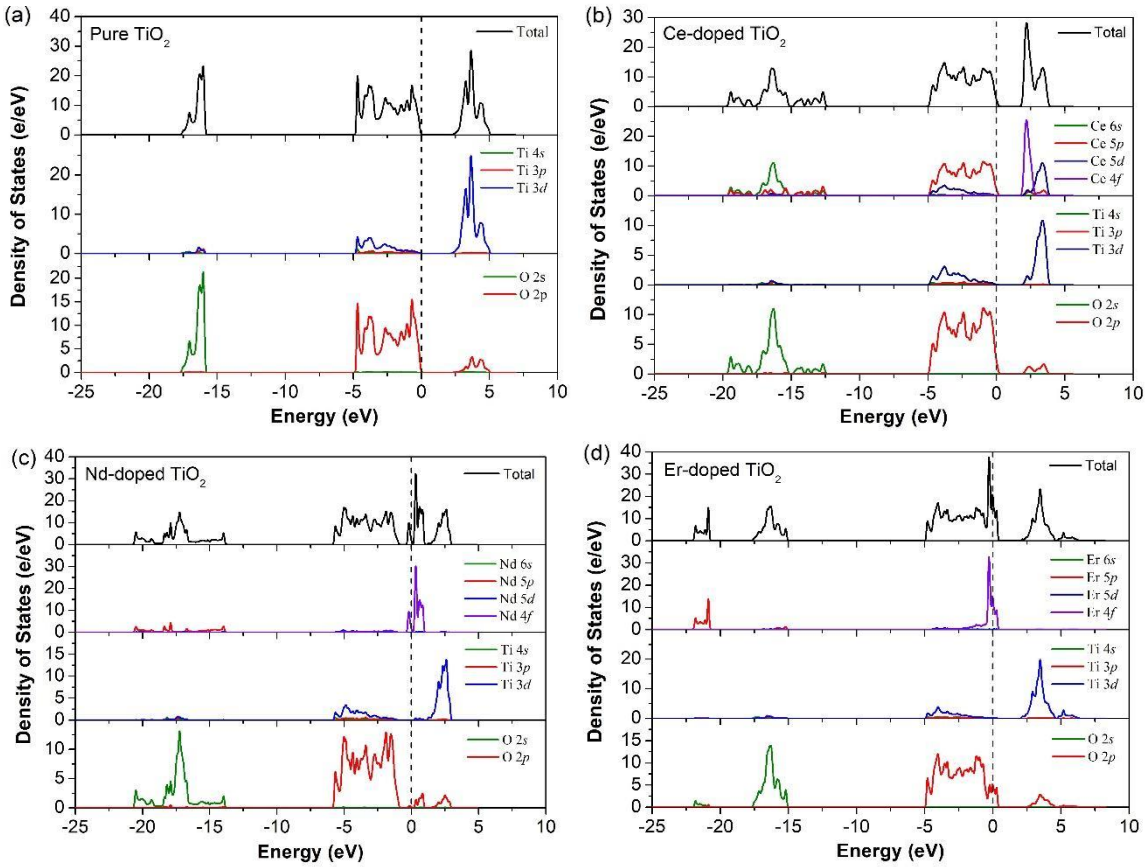

Figure 3. Total and partial density of states (DOS) of (a) pure TiO_2, (b) Ce- (c) Nd- and (d) Er-doped TiO_2.

3.1.3 Optical Properties

The absorption coefficients $\alpha(\omega)$ of pure TiO_2 and Ce-, Nd- and Er-doped TiO_2 against photon energy and wavelength are displayed in Figure 4. From the absorption coefficient versus energy, the absorption edges coincide with their respective band gap at the lower energy range. The absorption edges of all the Ln-doped TiO_2 shift toward longer wavelength region in visible light, which is called red shift. The red shift of absorption edge occurs due to the significant changes in electronic structures from the changing of composition of the energy bands, introduction of the impurity states and decreasing in the band gaps after Ln doping. So, the electrons in the valence band can be excited to the conduction band by absorption of the visible light. This will make the Ln doping are ideal to effectively utilize solar energy in the visible light region. The longer wavelength range in visible light comes from Nd-doped TiO_2 which has a major red shift compared to Ce- and Er-doped TiO_2, indicating the more sunlight can be absorbed by Nd-doped TiO_2. This situation means the Nd-doped TiO_2 possessed a narrower band gap that was good for absorbing sunlight. For Er-doped TiO_2, there is a great absorption coefficient in near-infrared

light (NIR) region which is due to its energy level transition. From the previous study, Liang et al. [32] reported that Er gives out reaction in the NIR region which confirms the ability of converting NIR light to visible light from upconversion luminescence process. The phenomenon of red shift is consistent with the results of Ln doping from Nd-doped ZnO by Wen et al. [33] which show that the optical absorption edge to shift towards low energy.

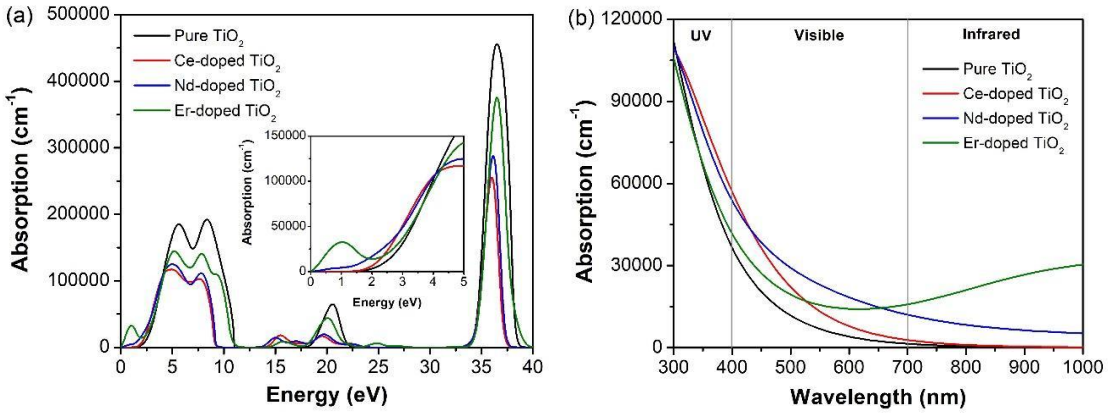

Figure 4. Absorption coefficient of pure TiO_2 and Ce-, Nd- and Er-doped TiO_2 against (a) energy (eV) and wavelength (nm).

4. CONCLUSION

In summary, the structural, electronic and optical properties of pure anatase TiO_2 and Ce-, Nd- and Er-doped anatase TiO_2 were calculated by first-principles calculations within the DFT method using the GGA-PBEsol functional. The effect of the Ln doping in TiO_2 alters the structural, electronic and optical properties of pure TiO_2. Due to the presence of 4*f* states belong to Ln elements, the band gaps of the Ln-doped TiO_2 become narrower compared to pure TiO_2. This band gap narrowing was primarily attributed to the substitutional Ln elements which introduced impurity energy levels (IELs) into the band gap of TiO_2. The calculated absorption coefficient of Ln-doped TiO_2 (Ln = Ce, Nd and Er) indicate that the doping cause red shift of absorption peak. Between Ce-, Nd- and Er-doped TiO_2, the wider shift of wavelength occurs for Nd-doped TiO_2 due to its smaller band gap. At the same time, the theoretical results provide useful data to explain the properties of Ln-doped TiO_2 (Ln = Ce, Nd and Er).

ACKNOWLEDGEMENTS

The authors would like to thank the Ministry of Higher Education (MOHE) Malaysia for funding this research under the FRGS grant 600-IRMI/FRGS 5/3 (121/2019) and Universiti Teknologi MARA (UiTM) for the facilities provided.

REFERENCES

[1] Tseng, T. K., Lin, Y. S., Chen, Y. J., Chu, H., Int. J. Mol. Sci. **11**, 6 (2010) 2336–2361.
[2] Haider, A. J., Jameel, Z. N., Al-Hussaini, I. H. M., Energy Procedia. **157** (2019) 17–29.
[3] Katal, R., Masudy-Panah, S., Tanhaei, M., Farahani, M. H. D. A., Jiangyong, H., Chem. Eng. J., **384** (2020) 123384.
[4] Roose, B., Pathak, S., Steiner, U., Chem. Soc. Rev. **44,** 22 (2015) 8326–8349.
[5] Luan, X., Wang, Y., J. Mater. Sci. Technol. **30,** 1 (2014) 1–7.

[6] Salvatori, P., Agrawal, S., Barreddi, C., Malapaka C., de Borniol, M., De Angelis. F., RSC Adv. **4,** 101 (2014) 57620–57628.
[7] Atabaev, T. S., Molkenova, A., Front. Mater. Sci. **13,** 4 (2019) 335–341.
[8] Llanos, J., Brito, I., Espinoza, D., Sekar, R., Manidurai, P., Soc. Open Sci. **5,** 2 (2018) 171054.
[9] Liu, M., Hou, Y., Qu, X., J. Mater. Res. **32**, 18 (2017) 3469–3476.
[10] Zalas, M., Klein, M., Int. J. Photoenergy. **2012** (2012) 1–8.
[11] Cavallo, C., Salleo, A., Gozzi, D., Di Pascasio, F., Quaranta, S., Panetta, R., Latini, A., Sci. Rep. **5** (2015) 16785.
[12] D'Souza, L. P., Shwetharani, R., Amoli, V., Fernando, C. A. N., Sinha, A. K., Balakrishna, R. G., Mater. Des. **104** (2016) 346–354.
[13] Sun, P., Liu, L., Cui, S. C., Liu, J. G., Catal. Letters **144,** 12 (2014) 2107–2113.
[14] Liang, J., Wang, J., Song, K., Wang, X., Yu, K., & Liang, C., J. Rare Earths **38,** 2 (2020) 148–156.
[15] Obregón, S., Colón, G., Chem. Commun. **48,** 63 (2012) 7865–7867.
[16] Perdew, J. P., Ruzsinszky, A., Csonka, G. I., Vydrov, O. A., Scuseria, G. E., Constantin, L. A., Zhou, X., Burke, K., Phys. Rev. Lett. **100,** 13 (2008) 136406.
[17] Clark, S. J., Segall, M. D., Pickard, C. J., Hasnip, P. J., Probert, M. I. J., Refson, K., Payne, M. C., Zeitschrift fur Krist. **220**, 5–6 (2005) 567–570.
[18] Horn, M., Meagher, E. P., Zeitschrift fur Krist. **136** (1972) 273–281.
[19] Arlt, T., Bermejo, M., Blanco, M. A., Gerward, L., Jiang, J. Z., Staun Olsen J., Recio, J. M., Phys. Rev. B. **61,** 21 (2000) 14414–14419.
[20] Mei, Z., Wang Y., Shang, S., Liu., Z., Inorg. Chem. **50**, 15 (2011) 6996–7003.
[21] Gao, P., Yang, L., Xiao, S., Wang, L., Guo, W., Lu, J., Materials (Basel). **12**, 5 (2019) 814.
[22] Clementi, E., Raimondi, D. L., Reinhardt, W. P., J. Chem. Phys. **47**, 4 (1967) 1300–1307.
[23] Philiips, J. C., Van Vechten, Chem. Phys. Lett. **5**, 3 (1970) 159–161.
[24] Zhang, J., Peng, W. Q., Chen, Z. H., Chen, H., Han, L. Y., J. Phys. Chem. C **116** (2012) 19182–19190.
[25] Mikami, M., Nakamura, S., Kitao, O., Arakawa, H., Gonze, X., Jpn. J. Appl. Phys **39,** 8 (2000) 847–850.
[26] Zhang, J., Zhou, P., Liu, J., Yu, J., Phys. Chem. Chem. Phys. **16,** 38 (2014) 20382–20386.
[27] Cui, Z.-H., Wu, F., Jiang, H., Phys. Chem. Chem. Phys. **18** (2016) 29914–29922.
[28] Reyes-Coronado, D., Rodríguez-Gattorno, G., Espinosa-Pesqueira, M. E., Cab, C., de Coss, R., Oskam, G., Nanotechnology **19,** 14 (2008) 145605.
[29] Kavan, L., Grätzel, M., Gilbert, S. E., Klemenz, C., Scheel, H. J., J. Am. Chem. Soc. **19**, 28 (1996) 6716–6723.
[30] Aryasetiawan, F., Karlsson, K., Jepsen, O., Schönberger, U., Phys. Rev. B - Condens. Matter Mater. Phys. **74**, 12 (2006) 1–9.
[31] V. I. Klimov, "Semiconductor and Metal Nanocrystals: Synthesis and Electronic and Optical Properties," in New York: Marcel Dekker, Inc., (2004) 1–22.
[32] Liang, L., Yulin, Y., Mi, Z., Ruiqing, F., Lele, Q., Xin, W., Lingyun, Z., Xuesong, Z., Jianglong, H., J. Solid State Chem. **198** (2013) 459–465.
[33] Wen, J. Q., Zhang, J. M., Chen, G. X., Wu, H., Yang, X., Phys. E Low-Dimensional Syst. Nanostructures **98** (2018) 168–173.